# A Comparative Study on Flexural Capacity of Reinforced Concrete Beams Reinforced with GFRP and Steel Bars

Muhammad Rafani[1], Tavio[1,*], Francisco Jose De Caso y Basalo[2]

[1]Department of Civil Engineering, Institut Teknologi Sepuluh Nopember, Surabaya, Indonesia

[2]Department of Civil and Architectural Engineering, University of Miami, Coral Gables, USA

Received 05 April 2026; received in revised form 01 June 2026; accepted 02 June 2026

DOI: https://doi.org/10.46604/aiti.2026.16342

## Abstract

This study compares the flexural capacity of reinforced concrete (RC) beams reinforced with glass fiber-reinforced polymer (GFRP) bars and conventional steel bars. It examines how reinforcement ratio affects relative moment-capacity performance. Twelve beam specimens are tested under four-point bending with reinforcement ratios from 0.5% to 2.4%. All specimens have identical geometry, transverse reinforcement, and loading configuration. Experimental moment capacities are calculated from ultimate loads and compared with Canadian Standards Association (CSA) S806-12-based predictions for GFRP-reinforced beams. At low reinforcement ratios ($\rho \leq 1.0\%$), GFRP-reinforced beams develop moment capacities comparable to or higher than steel-reinforced beams because of the high tensile strength of GFRP. At higher reinforcement ratios, steel-reinforced beams achieve larger capacities due to yielding and stress redistribution. The results indicate a gradual transition zone around $\rho \approx 1.1$-$1.2\%$, rather than a strict threshold. CSA predictions are generally conservative, except for the lowest-ratio GFRP specimen. These findings support comparative design.

**Keywords:** concrete beams, flexural capacity, GFRP reinforcement, moment capacity, sustainable infrastructure

## 1. Introduction

The increasing demand for durable and sustainable infrastructure drives the development of alternative reinforcement materials for reinforced concrete (RC) structures. Although conventional steel reinforcement is widely used due to its ductility and well-established mechanical performance, it remains highly susceptible to corrosion in aggressive environments. This susceptibility significantly reduces structural service life and leads to increased maintenance and rehabilitation costs [1-2].

Glass fiber reinforced polymer (GFRP) bars have emerged as a promising alternative owing to their high tensile strength, excellent corrosion resistance, and low self-weight [3-4]. These characteristics make GFRP particularly suitable for structures exposed to harsh environmental conditions, such as marine and industrial infrastructures. However, unlike steel, GFRP exhibits linear elastic behavior up to failure without yielding, resulting in brittle failure modes and limited ductility [5-6]. This fundamental difference significantly influences the flexural response and moment capacity of RC beams reinforced with GFRP.

Previous studies have extensively investigated the flexural performance of GFRP-reinforced concrete beams and consistently report notable differences compared to steel-reinforced members, particularly in terms of stiffness, crack width, and failure mechanisms [3, 7]. While several studies have demonstrated that GFRP-reinforced beams can achieve comparable flexural capacity at low reinforcement ratios, others have reported reduced flexural performance at higher reinforcement ratios due to premature concrete crushing or excessive deflection [8-9].

* Corresponding author. E-mail address: tavio@its.ac.id

Early experimental investigations confirm that GFRP bars can effectively function as internal reinforcement in concrete structures, demonstrating adequate strength and bond performance under flexural loading conditions [10-11]. Subsequent research has explored advanced applications, including hybrid reinforcement systems and improved confinement techniques, which enhance flexural performance and delay failure mechanisms [12-13].

The long-term durability of GFRP reinforcement has also been widely studied, particularly under alkaline exposure, sustained loading, and marine environments [14-15]. Environmental degradation mechanisms, such as chemical attack, moisture ingress, and alkalinity are identified as critical factors affecting long-term performance [16-17]. From a sustainability perspective, GFRP reinforcement attracts increasing attention due to its potential to reduce environmental impact and life-cycle costs compared to conventional steel reinforcement [18-19]. Nevertheless, challenges related to recycling and end-of-life management of fiber-reinforced polymer composites remain significant [20-22]. Life-cycle cost analyses further indicate that GFRP-reinforced systems can offer reduced maintenance and improved durability in aggressive environments [23-24]. Additional experimental studies on flexural behavior confirm that GFRP-reinforced beams exhibit distinct stiffness, cracking patterns, and failure characteristics compared to conventional steel-reinforced beams [25-26].

Despite the extensive body of research, many existing studies evaluate GFRP and steel reinforcement under different experimental conditions, including variations in geometry, material properties, and loading configurations. Such inconsistencies hinder direct comparison and lead to inconclusive or contradictory findings. In particular, there remains no clear consensus regarding the reinforcement ratio at which GFRP-reinforced beams transition from being competitive to inferior relative to steel-reinforced beams in terms of moment capacity. Therefore, the influence of reinforcement ratio on the comparative structural performance of GFRP and steel reinforcement has not yet been fully clarified.

To address this gap, the present study conducts a controlled experimental investigation on the flexural capacity of RC beams reinforced with GFRP and conventional steel bars under identical geometry, concrete strength, transverse reinforcement, and loading configuration. A total of twelve beam specimens, with reinforcement ratios ranging from 0.5% to 2.4%, are tested under four-point bending to enable a direct comparison of ultimate moment capacity and dominant observed failure characteristics. The contribution of this study is not the development of a universal design model, but a systematic experimental comparison that identifies a transition zone in relative moment-capacity performance between GFRP- and steel-reinforced beams. This scope is intentionally limited to the available experimental evidence and avoids implying a strict threshold or a general theory beyond the tested range.

The remainder of this paper is organized as follows. Section 2 describes the materials and experimental methods, including specimen preparation and test setup. Section 3 presents and discusses the experimental results, focusing on flexural performance, structural efficiency, and comparison with design code predictions. Finally, Section 4 summarizes the main conclusions and implications for structural design.

## 2. Materials and Methods

This section describes the materials, specimen configuration, loading setup, and data-analysis procedure used in the experimental program. It explains the reinforcement properties, concrete strength basis, beam geometry, and instrumentation so that the test conditions can be clearly understood. The same beam dimensions, transverse reinforcement, curing procedure, and four-point bending arrangement apply to both reinforcement groups. This consistency provides a controlled basis for comparing the GFRP- and steel-reinforced beams.

### *2.1. Material properties*

The mechanical properties of the reinforcement materials and concrete used in this study are determined based on manufacturer information and available standard test data. The ultimate tensile strength of the GFRP bars ranges from 656 to

765 MPa, depending on the bar diameter. Specifically, the tensile strengths ($f_{fu}$) are 765 MPa for 10 mm diameter bars (D10), 708 MPa for 13 mm bars (D13), 683 MPa for 16 mm bars (D16), and 656 MPa for 19 mm bars (D19). The steel reinforcement bars have a yield strength ($f_y$) of 420 MPa. All beams consist of normal-weight concrete with a target/available compressive strength value of 30 MPa for the moment-capacity calculations. As detailed batch-to-batch concrete strength statistics are unavailable, this limitation is explicitly acknowledged in the discussion.

### *2.2. Test specimens*

A total of twelve reinforced concrete beam specimens, each measuring 200 mm × 300 mm × 3000 mm, are fabricated and divided into two groups. Six beams contain GFRP bars, while the remaining six incorporate conventional steel bars. The beams are designed as singly reinforced members; therefore, no compression reinforcement is provided. This configuration focuses the comparison on the influence of tensile reinforcement type and reinforcement ratio. In both groups, the longitudinal reinforcement consists of bar diameters of 10 mm (D10), 13 mm (D13), 16 mm (D16), and 19 mm (D19), which achieve reinforcement ratios ranging from 0.5% to 2.4%. Fig. 1 illustrates the cross-sectional configuration and reinforcement layout of the specimens.

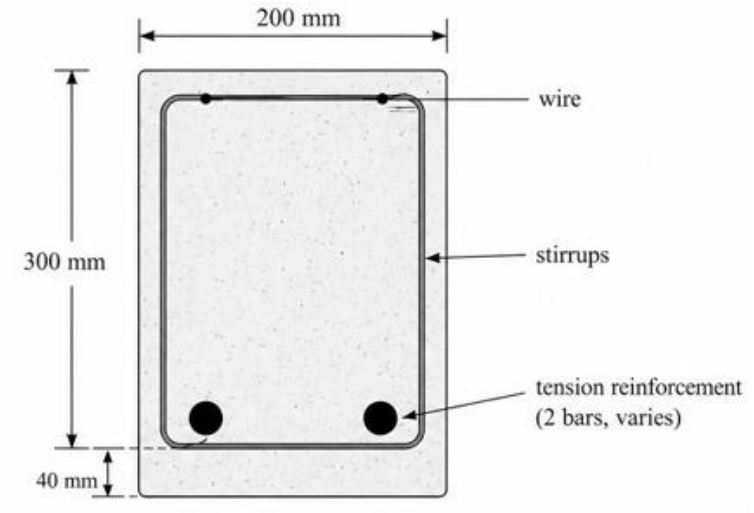


Fig. 1 Cross-sectional view and reinforcement details of the test beams

The specimen preparation process is illustrated in Figs. 2-3. Fig. 2 presents the casting procedure, during which particular attention is given to ensuring consistent geometry, accurate reinforcement placement, and proper concrete compaction for all specimens. Following casting, the beams undergo standard curing conditions, as shown in Fig. 3, to achieve the target concrete compressive strength of 30 MPa prior to testing. This controlled fabrication and curing process apply uniformly to both GFRP- and steel-reinforced beams to minimize variability and ensure a reliable comparison of structural performance.

Fig. 2 Casting process of the reinforced concrete beam specimens

Fig. 3 Curing process of the reinforced concrete beam specimens

The detailed characteristics of the beam specimens, including reinforcement type, geometric dimensions, longitudinal and transverse reinforcement configurations, and reinforcement ratios, are summarized in Table 1. All specimens possess identical cross-sectional dimensions and reinforcement layouts to ensure a consistent basis for comparison. The selected reinforcement ratios represent low, moderate, and high reinforcement levels, facilitating a comprehensive assessment of structural behavior across a wide range of conditions.

Table 1 Details of beam specimens

| Beam ID | Bars type | Dimensions (mm) ($b \times h \times L$) | Longitudinal reinforcement | Transverse reinforcement | Reinforcement ratio (%) |
|---|---|---|---|---|---|
| G-L2D13 | GFRP | 200 × 300 × 3000 | 2 D13 | D10 @100 mm | 0.5 |
| S-L2D13 | Steel | 200 × 300 × 3000 | 2 D13 | D10 @100 mm | 0.5 |
| G-L2D16 | GFRP | 200 × 300 × 3000 | 2 D16 | D10 @100 mm | 0.8 |
| S-L2D16 | Steel | 200 × 300 × 3000 | 2 D16 | D10 @100 mm | 0.8 |
| G-L4D13 | GFRP | 200 × 300 × 3000 | 4 D13 | D10 @100 mm | 1.1 |
| S-L4D13 | Steel | 200 × 300 × 3000 | 4 D13 | D10 @100 mm | 1.1 |
| G-L2D19 | GFRP | 200 × 300 × 3000 | 2 D19 | D10 @100 mm | 1.2 |
| S-L2D19 | Steel | 200 × 300 × 3000 | 2 D19 | D10 @100 mm | 1.2 |
| G-L4D16 | GFRP | 200 × 300 × 3000 | 4 D16 | D10 @100 mm | 1.7 |
| S-L4D16 | Steel | 200 × 300 × 3000 | 4 D16 | D10 @100 mm | 1.7 |
| G-L4D19 | GFRP | 200 × 300 × 3000 | 4 D19 | D10 @100 mm | 2.4 |
| S-L4D19 | Steel | 200 × 300 × 3000 | 4 D19 | D10 @100 mm | 2.4 |

### *2.3. Experimental setup and instrumentation*

Flexural testing proceeds using a four-point bending configuration to establish a constant moment region at the mid-span of each beam (Fig. 4). All specimens are simply supported, with a pinned support at one end and a roller support at the other, thereby ensuring statically determinate boundary conditions. The load applies monotonically using a hydraulic actuator and transfers through a spreader beam to produce two symmetrically placed concentrated loads. The magnitude of the applied load is continuously measured using a calibrated load cell. Deflections are recorded using linear variable differential transformers (LVDTs) installed at the mid-span and beneath the loading points to capture both maximum and localized deformations. All specimens are tested up to failure in order to capture ultimate load-carrying capacity and associated failure modes.

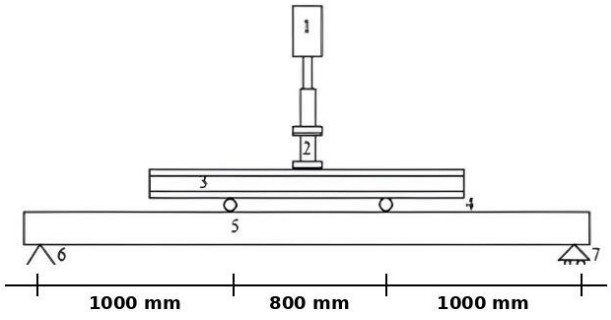


Fig. 4 Four-point bending test setup of the RC beam specimens

### *2.4. Data analysis*

The experimental nominal moment capacity ($M_{n,exp}$) of each beam is determined from the measured ultimate load using the four-point bending geometry. The predicted moment capacity ($M_{n,CSA}$) is calculated using a Canadian standards association (CSA) S806-12 [27]-based section-equilibrium approach for the GFRP-reinforced specimens. For clarity, the same CSA/reference capacity values are also shown together with the steel experimental results in Table 2 to support the comparative discussion. However, these values are not interpreted as a complete steel-code validation, as CSA S806-12 primarily addresses FRP-reinforced structures.

## 3. Results and Discussion

The nominal moment capacity ($M_n$) of the beam sections is determined based on internal force equilibrium and is expressed as:

$$M_n = T\left(d - \frac{a}{2}\right) \tag{1}$$

where $T$ is the tensile force in the reinforcement, $d$ is the effective depth, and $a$ is the depth of the equivalent rectangular stress block, defined as:

$$a = \beta_1 c \tag{2}$$

where $c$ is the neutral axis depth, and $\beta_1$ is the stress block parameter.

For GFRP-reinforced beams, the tensile force ($T$) is governed by the linear elastic behavior of the material:

$$T = A_f f_f \tag{3}$$

$$f_f = E_f \varepsilon_f \tag{4}$$

where $A_f$ is the cross-sectional area of GFRP bars, $f_f$ is the tensile stress in GFRP bars, subject to the ultimate tensile strength limit of the GFRP bars, $E_f$ is the modulus of elasticity of GFRP bars, and $\varepsilon_f$ is the tensile strain in GFRP bars.

These expressions describe the elastic tensile response of GFRP reinforcement before rupture. Unlike steel, GFRP does not yield; therefore, the stress in the bar depends on the strain developed in the section. This difference is important for interpreting the observed moment capacity and the reduced efficiency of GFRP at higher reinforcement ratios.

Conversely, for steel-reinforced beams, the tensile force ($T$) is calculated assuming yielding of the reinforcement:

$$T = A_s f_y \tag{5}$$

where $A_s$ is the cross-sectional steel area, and $f_y$ is the yield stress of steel bars.

For steel reinforcement, the yielding assumption represents the ability of the bars to develop plastic deformation and redistribute stress. This behavior provides a direct contrast with GFRP reinforcement, which remains linear elastic until failure. The comparison of these tensile-force models supports the later discussion on strength development, transition behavior, and structural efficiency.

The nominal moment capacity of the tested beams is evaluated based on the equilibrium of internal forces. The experimental results clearly demonstrate that the flexural performance is strongly influenced by both the type of reinforcement and the reinforcement ratio. The relationship between reinforcement ratio (e) and nominal moment capacity is presented in Fig. 5 for GFRP-reinforced beams and in Fig. 6 for steel-reinforced beams. These figures illustrate the variation in flexural capacity as a function of reinforcement percentage, enabling a direct comparison between the two reinforcement systems under identical testing conditions.

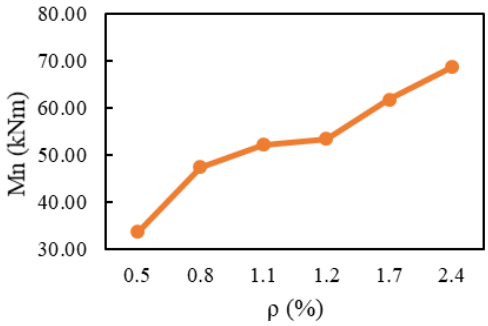


Fig. 5 Relationship between reinforcement ratio and nominal moment capacity of GFRP-RC beams

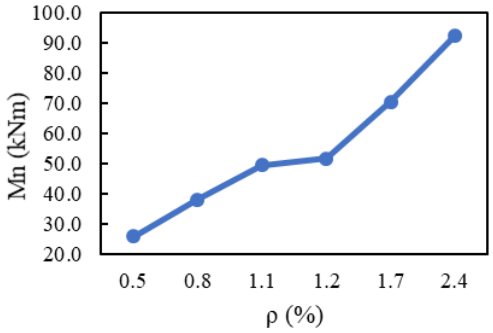


Fig. 6 Relationship between reinforcement ratio and nominal moment capacity of steel-RC beams

### *3.1. General behavior and moment capacity*

The nominal moment capacity of the tested beams is evaluated based on the measured ultimate load and internal force equilibrium. The experimental results indicate that both GFRP- and steel-reinforced beams exhibit an increasing trend in moment capacity with increasing reinforcement ratio. For GFRP-reinforced beams, the moment capacity increases from 33.74 kN·m at $\rho$ = 0.5% to 68.72 kN·m at $\rho$ = 2.4%. Similarly, steel-reinforced beams show an increase from 25.93 kN·m to 92.31 kN·m over the same range.

Although both reinforcement systems show similar increasing trends, their rates of increase differ. The difference becomes more pronounced at higher reinforcement ratios, indicating that the flexural response is governed not only by reinforcement amount but also by material behavior. This trend suggests that additional GFRP reinforcement becomes less effective in increasing flexural capacity at higher reinforcement levels.

This behavior is attributed to the inherent material characteristics of GFRP, particularly its relatively low modulus of elasticity, which leads to higher tensile strains and increased deflection under loading. Consequently, strain incompatibility between the concrete and the GFRP reinforcement becomes more pronounced, limiting the efficient utilization of the additional reinforcement. Furthermore, excessive deflection and serviceability constraints tend to govern the structural response at higher reinforcement ratios, thereby reducing the marginal benefit of increasing reinforcement content.

This observed reduction in effectiveness is consistent with previous analytical and experimental studies. These studies emphasize stiffness limitations, strain incompatibility, and deflection-controlled behavior as key factors influencing the performance of GFRP-RC beams, particularly at higher reinforcement ratios [28-30].

### *3.2. Comparative performance between GFRP and steel reinforcement*

A direct comparison between GFRP- and steel-reinforced beams reveals that the relative performance depends strongly on the reinforcement ratio. As shown in Figs. 5-6, at lower reinforcement ratios ($\rho \leq 1.0\%$), the GFRP-reinforced beams exhibit moment capacities comparable to or slightly higher than those of the steel-reinforced beams. This behavior is mainly attributed to the high tensile strength of GFRP reinforcement, which the system mobilizes effectively at lower reinforcement levels.

However, as the reinforcement ratio increases ($\rho \geq 1.2\%$), steel-reinforced beams demonstrate significantly higher moment capacities. This shift in performance is associated with the elastic–plastic behavior of steel, which allows stress redistribution after yielding. In contrast, the linear elastic behavior of GFRP leads to brittle failure without stress redistribution.

### *3.3. Transition zone in structural performance*

The experimental results suggest the presence of a transition zone in the range of approximately $\rho \approx 1.1$-1.2%, where the relative moment-capacity performance of GFRP- and steel-reinforced beams begins to shift. This transition zone does not represent a strict threshold or exact crossover point. At $\rho = 1.2\%$, the moment capacity of the GFRP-reinforced beam remains slightly higher than that of the corresponding steel specimen; however, beyond this range, the advantage shifts progressively toward steel reinforcement. Therefore, the concept of a transition zone provides a more accurate interpretation of the experimental data, reflecting a gradual change in governing behavior rather than a discrete boundary. This transition is primarily influenced by the change in failure mechanism, from tension-controlled behavior at lower reinforcement ratios to compression-controlled behavior at higher reinforcement ratios.

### *3.4. Structural efficiency and mechanical interpretation*

To further evaluate the relative performance, the ratio of moment capacity between GFRP- and steel-reinforced beams serves as an indicator of structural efficiency. At lower reinforcement ratios, the efficiency ratio is close to unity, indicating comparable structural performance. However, as the reinforcement ratio increases, the efficiency of GFRP decreases significantly, reaching approximately 0.70-0.75 at $\rho = 2.4\%$.

This reduction in efficiency can be attributed to three main mechanisms:

(1) Low modulus of elasticity: GFRP has a lower elastic modulus than steel; therefore, it develops higher tensile strain and larger deflection at the same load level. As a result, the additional reinforcement area is not converted into a proportional increase in flexural capacity at higher reinforcement ratios.

(2) Lack of stress redistribution: GFRP remains linear elastic up to rupture and does not exhibit yielding. Consequently, once the critical tensile or compression-zone limit is approached, the section has limited ability to redistribute stress, which contributes to a more brittle strength response.

(3) Neutral axis shift and lever-arm reduction: increasing the GFRP reinforcement ratio shifts the neutral axis upward and reduces the internal lever arm. The compression zone, therefore, becomes more influential, limiting the marginal increase in moment capacity obtained from additional GFRP reinforcement.

These factors collectively limit the effective utilization of additional GFRP reinforcement at higher reinforcement ratios.

### *3.5. Comparison with CSA S806-12 predictions*

To evaluate the applicability of the CSA S806-12-based prediction, the experimentally obtained moment capacities are compared with the corresponding calculated capacities. The CSA predictions for GFRP-reinforced beams are presented in Fig. 7, while Fig. 8 shows the experimental GFRP and steel results together with the same CSA reference curve to clarify the comparative trend.

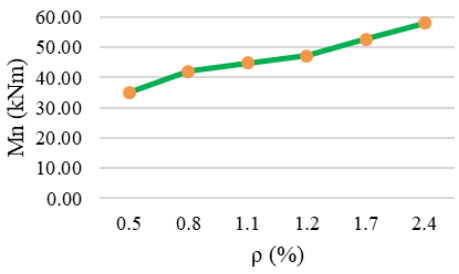


Fig. 7 Nominal moment capacity of GFRP-RC beams predicted by CSA S806-12

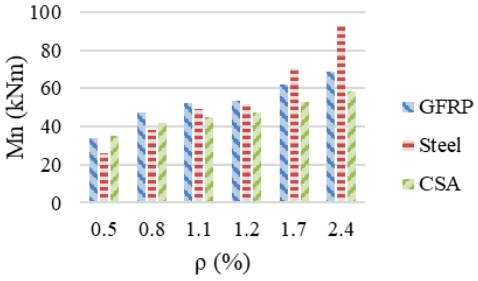


Fig. 8 Comparison of nominal moment capacity between GFRP- and steel-RC beams and CSA S806-12 predictions

The comparison between experimental results and CSA S806-12-based predictions indicates that the provisions generally provide conservative estimates for most GFRP-reinforced beams. The ratio of experimental-to-predicted moment capacity ($M_{n,exp}/M_{n,CSA}$) is greater than unity for most GFRP specimens, although the lowest-ratio specimen is slightly below unity. Therefore, the prediction should be described as generally conservative rather than uniformly conservative.

For the steel-reinforced beams, the CSA reference values are included only as a comparative baseline because CSA S806-12 is primarily intended for FRP-reinforced structures. The steel results are therefore interpreted in relation to the experimental GFRP trend rather than as a formal CSA validation for steel reinforcement. The differences between the GFRP and steel experimental trends are mainly caused by the different material responses: steel can yield and redistribute stress, whereas GFRP remains linear elastic up to rupture and is more strongly affected by stiffness and serviceability limitations.

*3.6 Failure modes and behavioral characteristics*

The typical failure conditions of the tested specimens following the flexural tests are presented in Figs. 9-10. Fig. 9 illustrates a representative beam reinforced with GFRP bars, while Fig. 10 shows a corresponding beam reinforced with steel bars. Distinct differences in crack patterns and failure modes emerge between the two reinforcement types, reflecting their fundamentally different mechanical behaviors. GFRP-reinforced beams exhibit relatively brittle failure characteristics, characterized by sudden rupture or concrete crushing with limited deformation capacity. In contrast, steel-reinforced beams demonstrate more ductile behavior, with noticeable yielding and larger deflections prior to ultimate failure.

Fig. 9 Typical failure mode of GFRP-reinforced beam after flexural testing

Fig. 10 Typical failure mode of steel-reinforced beam after flexural testing

Distinct differences in failure modes are observed between GFRP- and steel-reinforced beams. GFRP-reinforced beams exhibit relatively brittle failure, characterized by concrete crushing and/or sudden rupture of reinforcement without significant warning. In contrast, steel-reinforced beams demonstrate more ductile behavior, with yielding of reinforcement prior to failure. The dominant failure characteristics are identified based on visual observations and ultimate-load response. However, because strain gauges and crack-width instrumentation are absent, the failure-mode classification is interpreted as observation-based

rather than a complete strain-based classification for each specimen. Detailed strain measurements and crack-width data were not instrumented in this study. Therefore, all discussions related to stiffness, serviceability, strain distribution, crack width, and ductility are framed cautiously and are used only to support qualitative interpretation of the observed capacity and failure trends.

### *3.7. Influence of experimental variables and limitations*

Although the reinforcement ratio is considered the primary comparison parameter, it was not varied as a fully independent variable. The target reinforcement ratios are obtained through practical changes in bar diameter and/or number of bars. Consequently, secondary variables, such as GFRP tensile strength, bar spacing, bond characteristics, and effective stress development, may also influence the observed trends. Accordingly, the observed trends are interpreted as representative of practical design scenarios rather than strictly controlled parametric relationships.

In addition, the study is based on a limited number of specimens, and statistical variability is not explicitly evaluated. Therefore, the results are considered indicative for the tested specimen configuration rather than statistically generalized. Future studies should incorporate replicate specimens, broader reinforcement configurations, and uncertainty analysis to validate and extend the present findings.

### *3.8. Limitations, design implications, and future research*

The results indicate that GFRP reinforcement provides competitive flexural capacity at lower reinforcement ratios, particularly in applications where corrosion resistance is critical. However, its efficiency decreases at higher reinforcement ratios due to stiffness limitations, the absence of yielding, and brittle failure characteristics. Furthermore, since the tested beams lack compression reinforcement, the influence of compression steel on the transition remains outside the scope of this study. Future research focuses on the following targeted directions:

(1) Instrumentation Enhancement: Future tests should include strain gauges on concrete and reinforcement, LVDTs at key positions, and crack-width monitoring so that capacity trends can be directly connected to strain distribution, stiffness degradation, and serviceability response.
(2) Hybrid Reinforcement Systems: Steel-GFRP hybrid layouts and mixed tension/compression reinforcement require investigation to balance corrosion resistance, stiffness, ductility, and ultimate strength.
(3) Analytical and Empirical Modeling: Larger experimental databases are developed to calibrate transition-zone models that consider reinforcement ratio, elastic modulus, bar diameter, bond characteristics, and concrete strength.
(4) Compression Reinforcement and Section Configuration: Doubly reinforced sections and varying compression reinforcement ratios merit testing to quantify their influence on neutral-axis depth, compression-controlled behavior, and GFRP-to-steel efficiency.

These future studies are necessary because the present work is limited to twelve specimens without detailed strain or crack-width measurements. Additional instrumentation would allow the proposed transition zone to be validated more rigorously and connected to serviceability limits. A broader database would support the calibration of analytical or empirical models for different reinforcement layouts, hybrid reinforcement systems, and environmental exposure conditions. Such studies would improve the reliability of GFRP-RC design recommendations beyond the experimental range examined in the present work.

### *3.9. Summary of experimental-to-predicted ratios*

To summarize the comparative performance, Table 2 presents the experimental moment capacity, the CSA-based/reference capacity, the experimental-to-predicted ratio, and the GFRP-to-steel moment-capacity ratio for each reinforcement level. The relative performance ratio ($\eta$) is defined as:

$$\eta = \frac{M_{n,GFRP}}{M_{n,steel}} \tag{6}$$

where $M_{n,GFRP}$ is the nominal moment capacity of GFRP-reinforced concrete beam, and $M_{n,steel}$ is the nominal moment capacity of steel-reinforced concrete beam.

At low reinforcement ratios, the GFRP-to-steel moment-capacity ratio approaches or outperforms unity, confirming that GFRP reinforcement is structurally competitive in this range. As the reinforcement ratio increases, the ratio decreases to 0.744 at $\rho$ = 2.4%, indicating the reduced flexural efficiency of GFRP compared with steel at higher reinforcement levels.

This reduction in efficiency is associated with the lower modulus of elasticity of GFRP, the absence of yielding and stress redistribution, and the tendency for serviceability and compression-zone behavior to control the response.

The transition zone around $\rho \approx$1.1-1.2%, therefore, represents a gradual shift in relative performance rather than a discrete threshold. This interpretation aligns with the experimental observation that the GFRP specimen at $\rho$ = 1.2% still slightly exceeds the corresponding steel specimen, while steel becomes more advantageous at higher reinforcement ratios.

The ratios in Table 2 are interpreted together with the stated limitations of the study, particularly the limited number of specimens and the fact that reinforcement ratio is varied through practical changes in bar diameter and number of bars. The GFRP-to-steel ratio is used only as a comparative efficiency index for specimens with the same nominal reinforcement ratio. A value greater than 1.0 indicates that the GFRP-reinforced beam developed a higher experimental moment capacity than the steel-reinforced beam, whereas a value below 1.0 indicates the opposite. This interpretation separates the experimental GFRP-to-steel comparison from the CSA-based prediction check.

As shown in Table 2, the CSA-based prediction generally provides safe estimates for the GFRP-reinforced beams, with $M_{n,exp}/M_{n,CSA}$ values greater than unity for most specimens. The first GFRP specimen falls below unity, indicating that the prediction is not uniformly conservative across all reinforcement levels. For steel-reinforced beams, the table serves only as a comparative reference. A separate steel-specific design-code evaluation is required before drawing firm conclusions regarding the accuracy of code predictions for conventional steel-reinforced members.

The interpretation remains consistent with previous studies reporting that GFRP-reinforced beams may achieve competitive strength at lower reinforcement ratios. However, their efficiency can decrease at higher reinforcement ratios because of lower elastic modulus, absence of yielding, stiffness limitations, and brittle failure characteristics [3, 4, 7-9]. Consequently, the present contribution is limited to a controlled experimental comparison within the tested range and should be understood as evidence of a gradual transition zone rather than a universal design boundary.

Table 2 Experimental moment capacities, CSA/reference predictions, and GFRP-to-steel ratios

| Beam ID | $\rho$ (%) | $M_{n,exp}$ (kN·m) | $M_{n,CSA/ref}$ (kN·m) | $M_{n,exp}/M_{n,CSA}$ | $M_{n,GFRP}/M_{n,steel}$ |
|---|---|---|---|---|---|
| G-L2D13 | 0.5 | 33.74 | 35.19 | 0.959 | 1.301 |
| S-L2D13 | 0.5 | 25.93 | 35.19 | 0.737 | - |
| G-L2D16 | 0.8 | 47.41 | 42.08 | 1.127 | 1.245 |
| S-L2D16 | 0.8 | 38.08 | 42.08 | 0.905 | - |
| G-L4D13 | 1.1 | 52.15 | 44.90 | 1.161 | 1.055 |
| S-L4D13 | 1.1 | 49.42 | 44.90 | 1.101 | - |
| G-L2D19 | 1.2 | 53.43 | 47.15 | 1.133 | 1.033 |
| S-L2D19 | 1.2 | 51.72 | 47.15 | 1.097 | - |
| G-L4D16 | 1.7 | 61.79 | 52.68 | 1.173 | 0.876 |
| S-L4D16 | 1.7 | 70.56 | 52.68 | 1.339 | - |
| G-L4D19 | 2.4 | 68.72 | 58.13 | 1.182 | 0.744 |
| S-L4D19 | 2.4 | 92.31 | 58.13 | 1.588 | - |

## 4. Conclusions

This study investigated the flexural capacity and failure characteristics of RC beams reinforced with GFRP bars, compared with steel reinforcement. Twelve specimens, with reinforcement ratios of 0.5% to 2.4%, were tested under four-point bending using identical geometry, concrete strength, transverse reinforcement, and loading configuration. The results were evaluated against CSA S806-12-based predictions for GFRP-reinforced beams and compared with steel-reinforced specimens.

Based on the experimental investigation, the following conclusions are drawn:

(1) Comparative flexural performance: the reinforcement ratio ($\rho$) governs the relative performance of GFRP- and steel-reinforced beams. At lower reinforcement ratios ($\rho \leq 1.0\%$), GFRP-reinforced beams exhibit moment capacities comparable to, or slightly exceeding, steel-reinforced beams due to the high tensile strength of GFRP. However, beyond approximately $\rho \approx 1.1$-1.2%, lower modulus of elasticity of GFRP reduces flexural efficiency relative to steel sections.

(2) Failure mode characteristics: GFRP-reinforced beams exhibit brittle, compression-controlled failure governed by concrete crushing or sudden reinforcement rupture, with limited warning. In contrast, steel-reinforced beams demonstrate ductile behavior characterized by reinforcement yielding and significant deformation capacity.

(3) Validation of design provisions: the CSA S806-12-based predictions show generally conservative agreement with the experimental results for most GFRP-reinforced beams, although the lowest-ratio specimen was slightly unconservative. The steel-reinforced beams should be interpreted as references rather than full steel-code validation.

(4) Structural efficiency and transition behavior: a transition zone exists around $\rho \approx 1.1$-1.2%, where the relative moment-capacity advantage begins to shift from GFRP to steel reinforcement. This transition is gradual, not a strict threshold, because the GFRP specimen at $\rho = 1.2\%$ still slightly exceeds the corresponding steel specimen.

(5) Design implications: although GFRP reinforcement offers corrosion resistance and durability, its structural efficiency is strongly influenced by stiffness limitations and reinforcement ratio. Therefore, reinforcement type should be selected by considering environmental exposure, strength demand, serviceability requirements, and ductility expectations.

In summary, GFRP reinforcement represents a viable solution for aggressive environments. However, its efficiency depends on reinforcement ratio, stiffness, and serviceability. The findings should be interpreted within the limitations of the specimens, absence of strain/crack-width measurements, and lack of statistical uncertainty analysis.

## Acknowledgments

This research was made possible due to financial support from the Directorate of Research and Public Services, Institut Teknologi Sepuluh Nopember (ITS), through Research Grant ITS Batch 2 (Contract No: 1638/PKS/ITS/2024). The authors gratefully acknowledge financial support from the Institut Teknologi Sepuluh Nopember for this work, under the project scheme of the Publication Writing and IPR Incentive Program (PPHKI) 2025.

## Conflicts of Interest

The authors declare no conflict of interest.

## References

[1] B. Benmokrane, S. Mousa, K. Mohamed, and M. S. Ahmed, “Physical, Mechanical, and Durability Characteristics of Newly Developed Thermoplastic GFRP Bars for Reinforcing Concrete Structures,” Construction and Building Materials, vol. 276, article no. 122200, 2021.

[2] ACI Committee 440.1R-15, Guide for the Design and Construction of Structural Concrete Reinforced with Fiber-Reinforced Polymer (FRP) Bars, Farmington Hills, MI: American Concrete Institute, 2015.

[3] O. I. Abdelkarim, E. A. Ahmed, H. M. Mohamed, and B. Benmokrane, "Flexural Strength and Serviceability Evaluation of Concrete Beams Reinforced with Deformed GFRP Bars," Engineering Structures, vol. 186, pp. 282-296, 2019.

[4] W. Xue, F. Peng, and Q. Zheng, "Design Equations for Flexural Capacity of Concrete Beams Reinforced with Glass Fiber–Reinforced Polymer Bars," Journal of Composites for Construction, vol. 20, no. 3, article no. 04015069, 2016.

[5] R. H. P. Akhmad and Tavio, "Influence of Seawater on Strength of Concrete Beams Strengthened with Glass Fiber Reinforced Polymer Sheet," International Journal of GEOMATE, vol. 26, no. 117, pp. 35-42, 2024.

[6] C. Barris, L. Torres, C. Miàs, and I. Vilanova, "Design of FRP Reinforced Concrete Beams for Serviceability Requirements," Journal of Civil Engineering and Management, vol. 18, no. 6, pp. 843-857, 2012.

[7] C. Farias, S. Pessi, A. Wanderlind, J. H. Piva, and E. Pavei, "Flexural Behavior of Concrete Beams Reinforced with Glass Fiber Reinforced Polymer and Steel Bars," Revista de la Construcción, vol. 21, no. 3, pp. 506-522, 2022.

[8] M. Rafani, A. Suhardjono, Wisnumurti, A. Wibowo, and Tavio, "A Theoretical Study of GFRP RC Beams Deflection," Journal of Physics: Conference Series, vol. 1477, article no. 052047, 2020.

[9] O. Gouda, A. Hassanein, and K. Galal, "Experimental and Numerical Study on the Crack Width and Deflection Performance of GFRP Reinforced Concrete Beams," Engineering Structures, vol. 283, article no. 115721, 2023.

[10] S. H. Alsayed, Y. A. Al-Salloum, and T. H. Almusallam, "Performance of Glass Fiber Reinforced Plastic Bars as a Reinforcing Material for Concrete Structures," Composites Part B: Engineering, vol. 31, no. 6-7, pp. 555-567, 2000.

[11] R. J. A. Hamad, M. A. M. Johari, and R. H. Haddad, "Mechanical Properties and Bond Characteristics of Different Fiber Reinforced Polymer Rebars at Elevated Temperatures," Construction and Building Materials, vol. 142, pp. 521-535, 2017.

[12] X. Ruan, C. Lu, K. Xu, G. Xuan, and M. Ni, "Flexural Behavior and Serviceability of Concrete Beams Hybrid-Reinforced with GFRP Bars and Steel Bars," Composite Structures, vol. 235, article no. 111772, 2020.

[13] H.-L. Dong, W. Zhou, and Z. Wang, "Flexural Performance of Concrete Beams Reinforced with FRP Bars Grouted in Corrugated Sleeves," Composite Structures, vol. 215, pp. 49-59, 2019.

[14] C. Lu, Z. Qi, Y. Zheng, G. Xuan, and Y. Yan, "Long-Term Tensile Performance of GFRP Bars in Loaded Concrete and Aggressive Solutions," Journal of Building Engineering, vol. 64, article no. 105587, 2023.

[15] T. D'Antino, M. A. Pisani, and C. Poggi, "Effect of the Environment on the Performance of GFRP Reinforcing Bars," Composites Part B: Engineering, vol. 141, pp. 123-136, 2018.

[16] Y. Sun, Z. Jin, X. Zhang, and B. Pang, "Degradation of GFRP Bars in Alkaline Environments: An Experimental and Molecular Dynamics Study," Journal of Building Engineering, vol. 77, article no. 107449, 2023.

[17] D. Jia, Q. Guo, J. Mao, J. Lv, and Z. Yang, "Durability of Glass Fibre-Reinforced Polymer (GFRP) Bars Embedded in Concrete under Various Environments. I: Experiments and Analysis," Composite Structures, vol. 234, article no. 111687, 2020.

[18] S. Al Omar and A. Abdelhadi, "Comparative Life-Cycle Assessment of Steel and GFRP Rebars for Procurement Sustainability in the Construction Industry," Sustainability, vol. 16, no. 10, article no. 3899, 2024.

[19] S. Sbahieh, G. McKay, and S. G. Al-Ghamdi, "A Comparative Life Cycle Assessment of Fiber-Reinforced Polymers as a Sustainable Reinforcement Option in Concrete Beams," Frontiers in Built Environment, vol. 9, article no. 1194121, 2023.

[20] H. Fergani, M. Di Benedetti, C. M. Oller, C. Lynsdale, and M. Guadagnini, "Durability and Degradation Mechanisms of GFRP Reinforcement Subjected to Severe Environments and Sustained Stress," Construction and Building Materials, vol. 170, pp. 637-648, 2018.

[21] M. Inman, E. R. Thorhallsson, and K. Azrague, "A Mechanical and Environmental Assessment and Comparison of Basalt Fibre Reinforced Polymer (BFRP) Rebar and Steel Rebar in Concrete Beams," Energy Procedia, vol. 111, pp. 31-40, 2017.

[22] K. Pender and L. Yang, "Glass Fibre Composites Recycling Using the Fluidised Bed: A Comparative Study into the Carbon Footprint in the UK," Sustainability, vol. 16, no. 3, article no. 1016, 2024.

[23] G. Dhinakaran, S. Gowrisankar, and A. Jeyasehar, "Life Cycle Cost Analysis of Glass Fiber Reinforced Polymer Reinforced Concrete Beam," Asian Journal of Civil Engineering, vol. 17, no. 3, pp. 315–323, 2016.

[24] T. Cadenazzi, H. Lee, P. Suraneni, S. Nolan, and A. Nanni, "Evaluation of Probabilistic and Deterministic Life-Cycle Cost Analyses for Concrete Bridges Exposed to Chlorides," Cleaner Engineering and Technology, vol. 4, article no. 100247, 2021.

[25] H. Tran, T. Nguyen-Thoi, and H.-B. Dinh, "State-of-the-Art Review of Studies on the Flexural Behavior and Design of FRP-Reinforced Concrete Beams," Materials, vol. 18, no. 14, article no. 3295, 2025.

[26] H. Tran and T. Nguyen-Thoi, "Flexural Behavior of Beams Reinforced with FRP Bars: Test Database, Design Guideline Assessment, and Reliability Evaluation," Buildings, vol. 15, no. 18, article no. 3373, 2025.

[27] Canadian Standards Association, CSA S806:12 (R2021): Design and Construction of Building Structures with Fibre-Reinforced Polymers. Toronto, ON, Canada: CSA Group, 2012, reaffirmed 2021.

[28] Tavio, M. Rafani, I. G. P. Raka, and V. Ratnasari, "Flexural Capacity Predictions and Comparisons of GFRP Reinforced Beams," Journal of Physics: Conference Series, vol. 1477, article no. 052049, 2020.

[29] Z. Ummah and Tavio, "Proposed Formulation for Predicting Deflections of CFRP-RC Beams," International Journal of GEOMATE, vol. 25, no. 111, pp. 138-144, 2023.

[30] M. Rafani, Tavio, and F. J. D. C. Basalo, "Understanding Deflection in GFRP-RC Beams: A Systematic Review of Parameters, Models, and Code Implications," Civil Engineering and Architecture, vol. 14, no. 1, pp. 82-90, 2026.